Bioinspired and Biomimetic Membranes Using Ion Channel Pro-teins and Designer Peptides Conjugated With Graphene Oxide for Selective Ion Transport

Sanju Gupta *, Taylor Robinson , Brendan Evans

Posted Date: 26 April 2023

doi: 10.20944/preprints202304.0977.v1

Keywords: Bioinspired membranes; Graphene oxide; Pore channel proteins; Peptide; Diffusion; Ion selectivity.

Article

Bioinspired and Biomimetic Membranes Using ion Channel Proteins and Designer Peptides Conjugated with Graphene Oxide for Selective Ion Transport

S. Gupta [1,2,3,*], T. Robinson [2] and B. Evans [2]

[1] Department of Materials Science and Engineering, Pennsylvania State University, University Park, PA 16802, USA
[2] Department of Physics and Astronomy, Western Kentucky University, Bowling Green, KY 42101, USA
[3] Biotechnology Center, Western Kentucky University, Bowling Green, KY 42101, USA
* Correspondence: sgup77@gmail.com

Abstract: Recent advances in synthetic membranes allow their use in fields as diverse as food and agriculture, biotechnology, industrial wastewater treatment, and potable water production. Among the newly developed technologies, nanofiltration and more particularly desalination of seawater is actively pursued. However, current solid-state membranes performance is limited, which calls for development of novel membranes offering high permeability (ion and water flux) and ion differentiation (selectivity), usually considered antagonist features. We report the development of nanoporous membranes made of solid-state polymer carbonate track-etched (PCTE) films in which biological ion channels such as Gramicidin A (GA), alpha-hemolysin (α-HL), and outer-membrane protein F (OmpF) aquaporin are confined and graphene oxide (GO) conjugated cobalt ion selective binding peptide motifs (Co_{pep}) are adsorbed, referring as bioinspired and biomimetic approaches, respectively. The solid-state nanoporous membranes are attracting widespread attention since they offer scalability, mechanical robustness, selectivity, controlled pore dimension and shape, for water sustainability. The ion permeability, ion diffusion coefficient and selective ion recognition are evaluated via nanofiltration, cell diffusion, and UV-Visible absorption spectroscopy to gain insights into the role of key performance parameters including effective ion confinement in track-etched pores, rich surface chemistry, and peptide-induced channel for selective ion transport. These findings provide new avenues for artificial ion channels by synergistic combination of eco-friendly material design such as GO enabled by bio-molecular recognition chemistry.

Keywords: bioinspired membranes; graphene oxide; pore channel proteins; peptide; diffusion; ion selectivity

1. Introduction

Water is the most precious resource for existence of our life (mankind) as well as indispensable component for food production (agriculture), industrial processes (energy production), and hygiene. Though more than 70% of the Earth is covered with water ('blue planet'), with increasing demands for freshwater and dwindling resources pose a global threat to sustainable development, resulting in water scarcity [1,2]. Freshwater is a renewable resource, but not always available where it needs to be and incurs stress across *food-energy-water* (FEW) nexus [3,4,5]. Thus, it necessitates coordinated innovative research and development efforts, with re-consideration of energy-efficient water filtration technologies related to materials that can mitigate environment pollution or address climate forecast affecting our nation and the world [6,7,8]. Current water purification technologies include reverse osmosis (RO), nanofiltration (NF), and recently resurged forward osmosis (FO) processes that utilize membranes to achieve significant removal of contaminants [9,10,11,12,13]. RO is a pressure-driven process where unwanted impurities is forced through a semi-permeable membrane, selectively transporting monovalent ions (Na^+, K^+, Cl^-) and water molecules while rejecting

multivalent ions, dissolved organic compounds and micro-organisms (e.g., bacteria) [3,14,15,16]. The membranes used are based on conventional thin film polymer (polyamide; PA, cellulose acetate; CA, polysulfone; PS), polymeric composites, and ceramics that have salient advantages such as good separation capability, structural stability (mechanical robustness), anti-biofouling, and wide pH tolerance [17,18,19]. Membranes that recognize and selectively transport specific molecular and ionic species are being actively pursued to meet the needs in food processing, treatment of wastewater, brackish water, chemical, biomedical, and pharmaceutical industries. Specifically, the ability that differentiates ions yet keeping high permeability is the basis for ion separation [20], biotechnology [21,22], nanomedicine [23], and water desalination [3,24,25].

Molecular separation and ion rejecting membranes are primarily based on unique pores that mimic efficient and water selective biological proteins such as Aquaporin-1 (AQP1). The key structural features that enable efficient transport in AQP1 is its hydrophobic and narrow 0.3 nm diameter channel, which forces water to translocate in a single-file arrangement. The limited success of efforts to create scalable AQP-based membranes motivated researchers to develop bioinspired artificial channels [26]. Similarly, it is well-known that the transport of ions through biological membranes made of phospholipid bilayers is well controlled through embedded proteins, so-called naturally occurring biological ion-channels exhibit outstanding permeability and selectivity properties. Central to the ion channel is selectivity filter 'nanogate' composed of short or long chain peptides (polypeptides), responsible for differentiation between ions that can be quickly transferred in or out of the cell [27,28,29,30]. Unfortunately, this remarkable property of the biological membranes cannot be easily transferred to abiotic systems and thus there are challenges to overcome this problem. First, the idea of supporting the biological membrane on nanoporous solid-state material was proposed [31]. Then, the use of supported synthetic polymer bilayer-like membrane are investigated [32]. For instance, Kumar et.al., [33] incorporated functional water channel protein Aquaporin Z in ABA copolymers and demonstrated the stability and functionality of the channel in the artificial environment. More recently, Gonzalez-Perez et.al., [34] constructed a biomimetic stable polymer membrane array including ion channel Gramicidin-A (GA). Despite this system of synthetic protein-polymer membrane turning out to be more stable than biological membranes which is encouraging for further investigations, it is devoid of mechanical robustness to be utilized for practical applications.

Synthetic solid-state membranes offer advantages unparalleled to bilayer approaches, including chemical and mechanical stability, modified surfaces for desired functions, control over pore dimension and shape [35, 36]. Track-etched polymer membranes (PCTE)—polyimide (PI) or polycarbonate (PC)—with cylindrical nanopores are used as solid support and loading biological channels has been investigated yet with partial success. Second, building of mechanically stronger systems with surface functionality accomplished by immobilization of functional ligands mimicking ion channel properties performed by covalent attachment, hydrophobic interaction and electrostatic self-assembly of the ligands with active chemical sites on the pristine nanochannel surface have been explored. Thus, biomimetic approaches that combine bioinspired functional molecules with modifiable surface on solid supports offer great potential mimicking the functions and principles of biological ion channels. Additionally, key insights are looking at the individual components and their interactions to understand the behavior of membranes in the water filtration process. With reasonable understanding of such complex systems, the next step is to design better membranes and develop understanding of membrane processes. To this end, graphene oxide, GO (graphene layer with oxygen/hydroxyl functional groups at basal and edge planes) is an emergent material for solid-state membrane and selective ion transport through stacked GO layers with holes in the basal plane and interlayer spacing has been reported [14,37,38,39]. It was first realized by molecular dynamic (MD) simulations where nanopores were theorized on the graphene monolayer (basal plane) to allow water to permeate while rejecting or retaining undesired substances proficiently [24,24,40]. Since the oxygen containing groups (hydroxyl, epoxy, and carboxyl) at basal or edge plane sites offer rich surface chemistry, GO is a suitable scaffold for equipping functional ligands [41,42]. In general, the chemical functionality on channel forming pore surface determine the ion selectivity, which depends upon the

interaction between ligands on channel wall and molecules or solvated ions [43]. Most artificial ion channels relied on electrostatic [44,45] or size sieving mechanism [46] and for selective transport of molecules, molecular recognition chemistry has been applied for enantiomeric drugs [20] and complementary drugs [47]. However, selective ion transport based on recognition chemistry is much less explored [48,49].

In the present work, we adopted two related approaches namely, preparation of bioinspired (artificial ion channel proteins) and biomimetic (ion recognizable short chain peptide motifs) membranes in which corresponding biomolecules are confined within polymer track etched nanopores (thickness 2 micron and diameter 30 nm) that is conjugated with GO film as selective filter. Specifically, we report the hybrid bio-membranes with cylindrical nanopores filled with Gramicidin-A (GA; protein1), α-Hemolysin (α-HL; protein2) and outer membrane protein F (OmpF; protein3) verified using vibrational and confocal fluorescence spectroscopy. Then, the effective ion diffusion coefficient through hybrid membranes is determined by means of diffusion cell measurements of various mono- and bi-valent electrolytes i.e., Na^+, K^+, Ca^{2+}, and Mg^{2+} chloride solutions. Comparison of ion diffusion coefficient with protein-free membranes confirms the adsorption of these proteins within the channels and emphasizes that the diffusion increased significantly when effectively adsorbed. Briefly, GA is known to allow the transport of Na^+ and K^+ but tend to hinder divalent cations. This ionic artificial channel is the simplest and most studied by physiologists. It is a polypeptide constituted of 14 hydrophobic amino acids and in polar solvents it acquires β-helical dimeric double stranded conformation which is responsible for ion channel formation across the lipid bilayer [32,50]. Likewise, α-HL is expressed as a water-soluble monomer (33.2 kDa), which assembles to form a membrane-bound heptameric pore that are stable under high salt concentration, temperature, pH, etc. It is a mushroom-shaped protein, and its' structure is divided into three sub-domains (cap, rim and stem/transmembrane) resolved by x-ray crystallography (PDB ID: 7AHL) [51]. OmpF is a general outer membrane protein forming porin consisting of 16 antiparallel β-strands forming a barrel and displays eight domains [52]. Thus, porins are β barrel proteins across cell membrane act as a pore mediating the non-specific diffusion of small solutes, ions, and amino acids molecules can diffuse. However, unlike other membrane transport proteins, porins are large enough to allow passive diffusion, i.e., channels that are specific to different types of molecules.

On the other hand, in approach 2, polypeptides biomolecules composed of sequence of amino acids that have inherent recognition properties [53,54], offer possibility for selective transport through the channels on which they are adsorbed or anchored. Peptide motifs with specific target affinity have been identified through extensive search in biopanning technique [55,56,57,58]. The Co^{2+} ion binding is a sequence of octapeptide: EPGHDAVP (Glu-Pro-Gly-His-Asp-Ala-Val-Pro), named Co_{pep}, (peptide1) has been previously screened [48,59]. Other peptide motifs designed are Na_{pep} (DKEADKEA; Asp-Lys-Glu-Ala-Asp-Lys-Glu-Ala) [peptide2] and RF_8 sequence RFRFRFRF (Arg-Phe-Arg-Phe-Arg-Phe-Arg-Phe) [peptide3]. To evaluate selective Co^{2+} ion transport, we immobilized these peptides on GO functionalized solid-state supports. The resulting GO conjugated membranes with ion recognizable peptides showed remarkable ion diffusion and effective transport of Co^{2+} ions that was reasonably selective over other transition metal ions as in the biological ion channels. Therefore, ion recognition capability of various peptide motifs successfully translates into ion specificity. This study provides novel ways for developing artificial ion channels via synergistic combination of biomimetic recognition chemistry, with GO as nanoplatform.

2. Experimental Section

2.1. Preparation of Track-Etched Polymer Membrane and Materials Dispersion

Synthesis of bioinspired membranes as in approach 1 begins with surface modification of commercial polycarbonate track-etched membrane (PCTE) supports from Whatman-Nucleopore (0.03-micron pore and 47 mm diameter) or from Sterlitech (0.03-micron pore and 43 mm diameter) and preparation of solutions following the sequence. To make 0.01 M solution of PVP, 278 mg of PVP polymer was dissolved in 250 mL DI (deionized) water. Then, eight electrolytes of varying

concentrations were made for diffusion cell tests including 0.5 g/L of NaCl, KCl, $CaCl_2$, and $MgCl_2$ as well as 0.01M and 0.1M concentrations of each $CoCl_2$ and $NiCl_2$ electrolytes. Then, 1.5 μM of GA in methanol was created. Dilution of 1.5 μM to 20 mL of 100 nM was achieved by adding 18.7 mL of methanol to 1.3 mL of 1.5 μM GA. Graphene oxide (GO) was prepared following modified Hummers' method [14,39]. The hydroxyl, ester, and epoxide groups were converted to carboxylic (-COOH) group by treating as-prepared GO with appropriate chemicals. To create a GA+GO solution, 16 mL of GO (70 μg/mL in DI) and 16 mL of GA (100 nM in methanol) were stirred together to create 32 mL of GA+GO dispersion. A total of 42 membranes were used, where in 36 were treated with 0.01M PVP that renders them hydrophobic with 6 left as-purchased (pristine). The membranes were left soaked in PVP for 25 minutes, and afterward the excess PVP solution was removed with a pipette. Then, 24 of the 36 PVP treated membranes were soaked in ethanol for 15 minutes. The nanopore diameter equals 30-40 nm and the nanopore density is about 10^8–$10^9/cm^2$.

2.2. Insertion of Artificial Ion Channel Proteins Inside Track-Etched membranes (Approach 1)

This subsection presents a scheme to synthesize bioinspired membranes with various biological ion channel proteins as solid-state nanopores. Prior to impregnation of nanoporous membranes with proteins, they were percolated with ethanol and then removed by water percolation as described above. This process partly degrades the hydrophobic external surface while not damaging the nanopores apparent from visual or SEM images. After the removal of excess ethanol, 12 membranes were treated with 100 nM GA in mixed water-ethanol (95/5), 12 membranes were treated with GA+GO, and left to soak for 3 days (72 hours) at room temperature. After soaking, 6 of the 12 GA-soaked membranes were given an additional layer of GA, making them double-layered GA membranes. They were washed and kept in pure water until further experiments. The same procedure was carried out to prepare membranes with other ion channel proteins.

To observe GA by confocal fluorescence spectroscopy, fluorescent labeling was carried out with Alexa-fluor 594 succinimidyl-ester (Invitrogen®) in ethanol and the mixture was stirred for an hour followed by removal of ethanol by evaporation under vacuum. The suspension of proteins obtained after water addition is filtered on Millipore membrane to remove Alexa-fluor 594 excess. Ultrapure water from milliQ 18MΩ is used throughout this work. Also, the labeled GA protein trapped into millipore membrane can be retrieved by methanol washing. The UV-Visible spectroscopy yields the GA labeling ratio of 0.27. As for the confirmation of GA insertion inside the nanopore, either ethanol-treated or as-purchased PCTE membrane, the labeled solution is poured into a mixed water-methanol (95/5) solution containing 10^{-7} moles per liter of GA and is left for impregnation during 72 h at room temperature followed by washing.

2.3. Peptide-GO Conjugated Membrane Synthesis (Approach 2)

Firstly, PBS (phosphate buffer solution, pH 7.4) solution was diluted to a 1M concentration from 7M and then 50 mL of 10 mM EDC was created by dissolving 96 mg in 50 mL of 1M PBS buffer, and 2.5 mM NHS was created by dissolving 14 mg in 50 mL of 1M PBS buffer. Then, the 2 g/L GO solution in DI was diluted by adding 37.5 mL of DI to 12.5 mL of 2 g/L GO solution. Therefore, a 0.5 g/L GO solution in DI was created. NHS solution (25 mL), EDC solution (25 mL), and GO solution (50 mL) were mixed using a magnetic stirrer for 15 minutes obtaining 100 mL solution. The solution was then ultrasonicated for 1 hour and stirred again with a magnetic stirrer for 10 minutes. After the GO-COOH was prepared, solutions of three peptides and two proteins were prepared using 1M PBS buffer as solvent. They include protein 2 (α-HL) solution adding 40 mL of 1M PBS buffer to the total amount to obtain 0.378 mM (or 90 μM) solution. Protein 3 (OmpF) was made into a solution by adding 40 mL of 1 M PBS buffer to the total amount to get 3.8 μM (or 0.9 μM) solution. The same was done for peptide 1 (Co_{pep}), peptide 2 (Na_{pep}) and peptide 3 (RF_8) to obtain 0.116mM (or 30 μM), 0.1mM (25 μM), and 0.11 mM (22 μM) solutions in 1M PBS buffer respectively. Then, 30 mL (or 6 mL) of the peptide and protein solutions were individually mixed with 10 mL (or 2 mL) of 0.5 g/L (0r 0.1 g/L) GO-COOH, and ultrasonicated for 1 hour. More solutions were prepared as before to create two sets of membranes for reproducibility.

Preprints (www.preprints.org) | NOT PEER-REVIEWED | Posted: 26 April 2023 doi:10.20944/preprints202304.0977.v1

MCE (mixed cellulose ester) membranes were placed in individual petri dishes with cut-out filters and treated with each peptide and protein solution with added GO-COOH prepared above and left to sit for a day (24 h). Then, the excess solution was removed and left to sit for another day to dry. The prepared GO or GO-COOH and GO-peptide solutions were vacuum-filtered through MCE membranes and the loading amount was ~0.1 mg.cm^{-2} eventually preparing MCE membranes for the second approach. Figure 1 shows schematic illustration of the two approaches studied in this work.

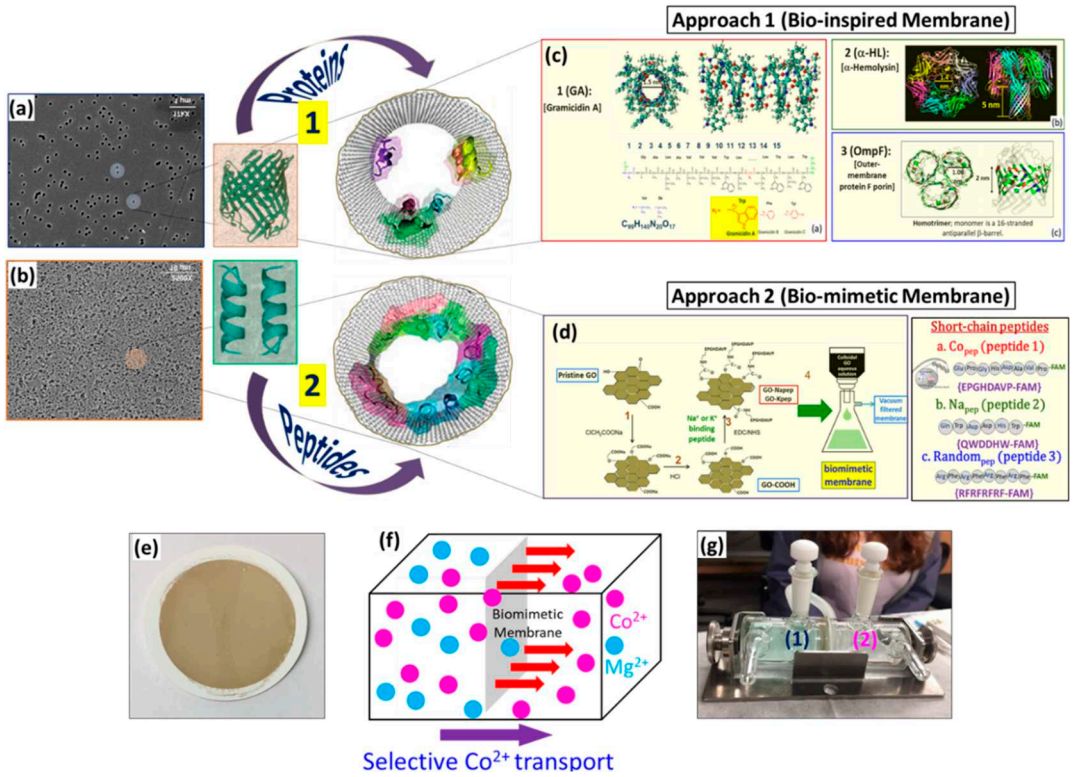

Figure 1. FE-SEM of pristine (a) polycarbonate track etched (PCTE) and (b) mixed cellulose ester (MCE) membranes. (c) PCTE treated with PVP (polyvinyl pyrrolidone) and ethanol in which three different ion channels (GA, α-HL, OmpF) confined are realized–Approach 1 (bioinspired). (d) Fabrication steps for MCE supported GO-conjugated Co$_{pep}$, Na$_{pep}$ and RF$_8$ membranes–Approach 2 (biomimetic). Typical conformations of GA and peptide1 conjugated GO inside the nanopores are also shown. (e) A photograph of GO–Co$_{pep}$ membrane on MCE support filter. (f) A diagram of ion diffusion and (g) a commercial diffusion cell used for membrane transport tests showing (1) chloride electrolyte and (2) pure water compartments.

2.4. Membranes Characterization

The membranes were characterized to reveal surface morphology, microstructure, surface chemistry, and lattice vibration properties by electron microscopy, confocal fluorescence spectroscopy and Raman spectroscopy. Field emission scanning electron microscopy (FE-SEM; JEOL Model JSM-6510LV, MA) images were taken while operating at a primary electron acceleration voltage of 15 kV at constant current 45 μA in secondary electron imaging mode with a LaB_6 filament. Thin films were also created on cleaned SiO_2/Si substrates for GO (in DI, 0.5 g/L), GO-COOH (0.1 g/L), GA (1.5 μM in methanol), GA (100 nm in DI)+GO (70 μg/mL in DI), α-Hemolysin (in PBS, 0.756 mM), α-Hemolysin+GO-COOH (90 μM), OmpF+GO-COOH (0.9 μM), Peptide 1+GO-COOH (30 μM), Peptide 2+GO-COOH (25 μM), and Peptide 3+GO-COOH (25 μM). After depositing each of the samples on individual substrate and left drying for 24h, another layer was added and left for another 1 day. The films were stored in dry cool place and Raman spectra was acquired. They were measured using a micro-Raman spectrometer (Model InVia Renishaw *plc*, Hoffman Estates, IL, USA) equipped

Preprints (www.preprints.org) | NOT PEER-REVIEWED | Posted: 26 April 2023 doi:10.20944/preprints202304.0977.v1

with a laser providing excitation wavelength 633 nm. The scattered light from the sample is collected in backscattering geometry transmitted and detected by CCD camera. An objective lens of 50x was used providing a spot size of ~1–2 µm and the laser power on the sample is maintained at <0.5mW (5%) to avoid local heating effects. Raman spectra ranged from 120 cm^{-1} to 3200 cm^{-1} with spectral resolution 1 cm^{-1}. A UV–Visible spectrophotometer (PerkinElmer 1050) in a range of 200–700 nm was used to determine the proteins and peptides with and without GO conjugated solutions pre- and post-diffusion tests.

2.5. Membrane Performance (Ion Transport/Diffusion Tests and UV-Vis Absorption Spectroscopy)

The membranes performance is evaluated in terms of permeability, ion diffusion, selective ion rejection and using UV-Visible absorption spectroscopy to determine concentration post-diffusion for complementarity. Ion diffusion tests were undertaken using a commercial Side-Bi-Side Diffusion Cell (PermGear Inc. Hellertown, PA) with a hole 2.1 cm in diameter on the feed side compartment (1). The feed solution of the respective electrolyte was inserted using a pipette into chamber 1, and chamber 2 was filled with RO water permeate (see Figure 1g). Both chambers held up to 10 mL, but each were filled to about 9 mL. Initially, plain PCTE and MCE membranes were tested with eight different electrolytes: NaCl (0.5 g/L), KCl (0.5 g/L), $CaCl_2$ (0.5 g/L), $MgCl_2$ (0.5 g/L), $CoCl_2$ (0.01 M and 0.1 M) and $NiCl_2$ (0.01 M and 0.1 M). Membranes are cut to appropriate sizes, a white O-Ring held the membrane in place between the two chambers, a metal holder was used to hold the chambers together and increase the speed of diffusion by stirring. This configuration allowed for the diffusion of feed into permeation through respective membranes prepared in this study. The initial concentration of RO water was measured using a conductivity meter, as well as the initial conductivity of the electrolyte in the feed chamber. Initially, the conductivity in chamber 2 was measured every 30 minutes during tests, but the increments were decreased to 15 minutes for efficiency and to increase the number of data points for better statistics. We report effective ion diffusion coefficient D_{ion}^{mem} through as-purchased and ethanol-treated hybrid nanoporous membranes either impregnated (or not) with peptides/proteins. D_{ion}^{mem} is determined from diffusion cell experiments *albeit* indirectly from the ion flux passing through the membranes when placed between two compartments filled with a given electrolyte and pure water respectively. The quantity of the ions crossing membrane nanopores by unit time is determined by measuring the evolution of ionic conductivity $\sigma_{ion}^{(2)}$ in pure water compartment (note that the subscript (2) refers to pure water compartment and (1) to that of chloride electrolytes). Both the compartments are continuously stirred during the experiment. According to experimental conditions, D_{ion}^{mem} can be determined following mathematical treatment provided herein. The ionic conductivity in chamber 2 is given by: $\sigma_{ion}^{(2)} = \lambda_{cation} C_{cation}^{(2)} + \lambda_{anion} C_{anion}^{(2)}$, where λ is the molar conductivity and C the concentration. It can also be written from textbook as [60]:

$$C^{(2)} = \sigma_{ion}^{(2)}/\lambda_{elec}^{0} = (D_{ion}\ C^{(1)} A_m / V^{(2)}.\ d_m).t \text{ or } C^{(2)}/(C^{(1)} A_m / V^{(2)}.\ d_m) = D_{ion}.t \quad (1),$$

where A_m is membrane surface area, d_m membrane thickness, $V^{(2)}$ volume of compartment (2) and t the time following Fick's law of diffusion. Thus, the value of D_{ion} is calculated following linear relationship of concentration in compartment (2) with time (t) of diffusion cell measurements. Additionally, the relative ion permeability is given by:

$$P_{ion}^{rel} = P_{ion}^{mem}/D_{ion}^{bulk};\ P_{ion} = D_{ion} \times K \qquad (2),$$

where K is the partition (or distribution) coefficient. The corresponding D_{ion}^{bulk} $(cm^2.s^{-1})$ for Na^+ (1.50×10^{-4}), K^+ (1.95×10^{-5}), Ca^{2+} (7.93×10^{-6}), Mg^{2+} (7.05×10^{-6}), Co^{2+} (7.45×10^{-6}), Ni^{2+} (7.59×10^{-6}), and Cl^- (1.33×10^{-4}). The value of K can be determined by the shake flask method using two immiscible solvents [61]. The results showed that the presence of salt changes the partition coefficient such that it increased with salt concentration. The most common hydrophilic solvent is water (or phosphate buffer of pH 7.4) and for organic phase is octanol (or ethanol). For instance, the value of K at water-ethanol (or water-octanol) followed:

Preprints (www.preprints.org) | NOT PEER-REVIEWED | Posted: 26 April 2023 doi:10.20944/preprints202304.0977.v1

$$log\ P = logS_O - logS_w \qquad (3),$$

where S is the solubility in octanol (S_o) and water (S_w). For NaCl, KCl, $MgCl_2$, $CoCl_2$, and $NiCl_2$ the values result in 2.075×10^{-3}, 1.279×10^{-3}, 1.365×10^{-1}, 1.590×10^{-1}, and 1.18×10^{-1}, respectively.

We also report the permeability and salt rejection of the membranes examined by evaluating the selected mono- and di-valent (NaCl, KCl, $CaCl_2$, and $MgCl_2$) chloride electrolytes. To minimize the concentration polarization effect on the retention performance, the feed solution was continuously stirred at 500 rpm during the dead-end filtration (Model HP4750, Sterlitech Inc., Auburn, WA) described in detail elsewhere [14]. The retention performance of membranes for the electrolyte ions were calculated using equation:

$$R(\%) = \frac{C_f - C_p}{C_f} \times 100(\%) - (4),$$

where C_f feed and C_p permeate conductivity (or concentration), respectively. They were measured by ion conductivity meter (Cole-Palmer, Model Oakton CON 450 Meter). Likewise, surface adsorption is calculated using:

$$Ads.(\%) = \frac{V_f C_f - V_p C_p}{V_f C_f} \times 100(\%) - (5),$$

where V_f and V_p refer to volume of feed and permeate, respectively.

A UV–Visible spectrophotometer (Perkin-Elmer Model 1050) in 200–700 nm range and fluorescence spectra were used to determine the respective ion concentration of permeates. The $CoCl_2$ and $NiCl_2$ permeate samples obtained during diffusion cell tests involving the MCE membranes were organized following the sequence of measurements. For example, a plain MCE membrane tested with $CoCl_2$ (0.1 M) would have 10 individual vials of permeation: 10 min, 20 min, 30 min, 40 min, 50 min, 60 min, 70 min, 80 min, 90 min, and the final feed. Small volumes of the sets of samples, as well as small volumes of GO-COOH (0.1 g/L), GA (100 nM in ethanol/water mix), GA (100 nm in DI)+GO (70 µg/mL in DI), α-Hemolysin (in PBS, 0.756 mM), OmpF (0.91 mM), α-Hemolysin+GO-COOH (90 µM), OmpF+GO-COOH (0.9 µM), peptide1+GO-COOH (30 µM), and peptide2+GO-COOH (25 µM) were placed in a tray with 96 pockets, and labeled accordingly on a matrix. The Absorption was measured between 230–650 nm and the fluorescence were measured with excitation at 320 nm (or 430 nm) between 350–650 nm (or 480–650 nm) range. All statistical analysis was performed using Origin software *ver*. 21b. One-way analysis of variance (ANOVA) was performed for various comparison. The Levenberg–Marquardt algorithm as least-squares method was used to designate the statistical significance. Results were displayed as an average of four or five replicates that were conducted for reproducible results and p value of 0.05.

3. Results and Discussion

3.1. Morphological and other characterization of membranes

A series of field emission scanning electron microscopy (FE SEM) images are shown in Figure 1 revealing surface morphology of as-purchased PCTE (Figure 1a–c), PVP and ethanol treated (Figure 1d), GA impregnated (Figure 1e,f), GO-conjugated GA membrane (Figure 1g), GO-COOH layer morphology (Figure 1h), as-purchased MCE (Figure 1i,j), GO-conjugated peptide (Figure 1k,l), and proteins (Figure 1m,n) membranes. The surface modification at the surface and edges of nanopores in PCTE is apparent at various stages of processing without significant altering the pore structure and diameter. Likewise, the MCE membranes modified with peptide 1, peptide 2, protein 2 and protein 3 conjugated with GO present rougher surfaces. The interlayer GO distance increased upon insertion of peptides and proteins by almost 0.5 nm. Chemical phases of these membranes at various stages of processing and with different biological molecules were examined by confocal Raman spectroscopy (see Figure 1o). The spectra showed characteristic first-order D (disorder-activated) and G (graphitic or sp^2 C) Raman bands associated with GO and GO-COOH besides vibrational bands assigned to proteins and peptides as labeled. It is well-known that GO has many oxygenated surface

Preprints (www.preprints.org) | NOT PEER-REVIEWED | Posted: 26 April 2023 doi:10.20944/preprints202304.0977.v1

functional groups including hydroxyl (C-OH), epoxide (C-O-C), and carboxylic (-COOH) groups. It turns out that after proteins and peptides impregnation, the carbonyl C=O peaks around 1600 cm^{-1} were increased due to amide bonds and carboxylic groups in these biological molecules is the contributing factor. The presence of bands at lower wavenumbers around 200-600 cm^{-1} and higher wavenumbers at around 950 cm^{-1}, 1246 cm^{-1} and 1661 cm^{-1} confirm successful functionalization. For instance, in case of GO-Co_{pep} while the bands at 1660 cm^{-1} and 1246 cm^{-1} were assigned to stretching vibration of C-N and -CO-NH-, respectively, the band at around 900 cm^{-1} is associated with protein phosphate group PO_4^{2-}.

We attempted to measure the fluorescence response by confocal fluorescence spectroscopy to confirm the presence of labelled protein GA [62]. It allows to measure the fluorescence signal through the thickness of the membrane by steps of 0.2 µm. The fluorescent signal measured on the membrane surface revealed that the protein concentration is homogeneous throughout the sample. Fluorescence counts obtained are corrected by acquisition time and excitation power for statistics. Figure 1p reports the representative fluorescence signal response of the PCTE membrane with GA solution, inside the membrane, and membrane/solution interface. It is emphasized that the fluorescence intensity is about three and six times larger than in the solution. The intensity signals clearly point out that the concentration of GA is alike throughout the thin film thickness and GA is not strongly adsorbed at the polymer surface. These outcomes unambiguously indicate that GA is confined into the cylindrical nanopores of the polymer and that the treatment with ethanol increased the quantity of absorbed GA protein.

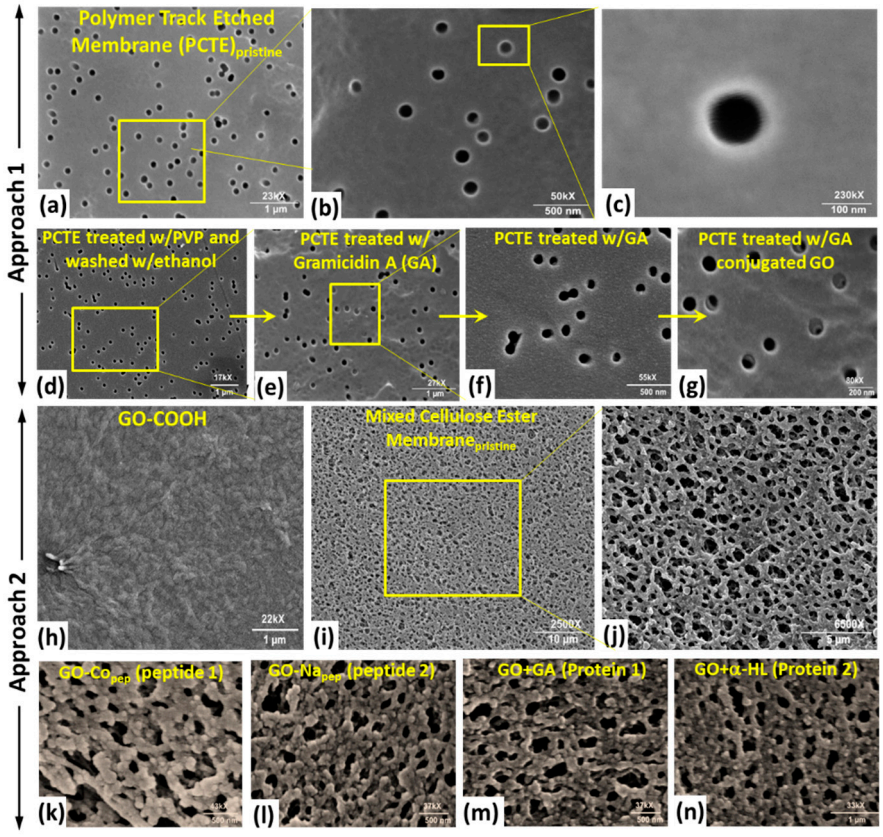

Preprints (www.preprints.org) | NOT PEER-REVIEWED | Posted: 26 April 2023 doi:10.20944/preprints202304.0977.v1

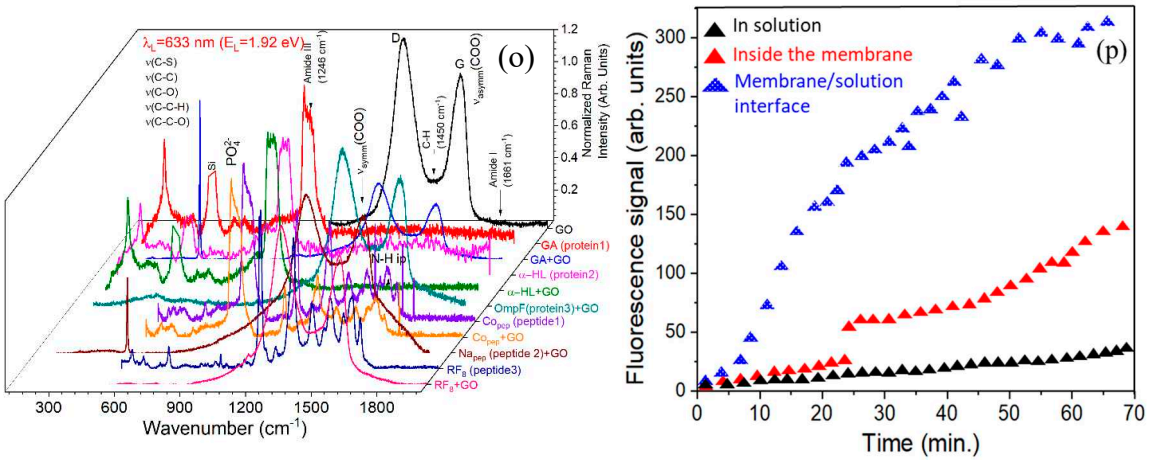

Figure 2. FE-SEM images of (a–g) pristine PCTE treated with PVP and ethanol and impregnated with ion channel GA as a representative example and GA conjugated with GO. (h) GO nanosheet. (i–n) pristine MCE membrane support at two magnifications and treated with peptide1, peptide2, protein1 and protein2 conjugated with GO. Scale bars are shown at the bottom of images. (o) Representative Raman spectra of membranes conjugated with and without GO showing characteristic vibrational peaks associated with different chemical bonding and functional groups. (p) Fluorescence signal as a function of time in labelled GA solution, inside the membrane and at membrane/solution interface.

3.2. Ion transport through artificial biological ion channel membranes and mechanistic aspects

Figure 3 shows the measured ionic conductivity evolution with time in compartment (2) during diffusion cell experiment for electrolytes containing mono- (NaCl, KCl) [Figure 3a,b] and di-valent ($CaCl_2$, $MgCl_2$) [Figure 3c,d] cations at concentration 0.5 $g.L^{-1}$ for PCTE membranes impregnated with GA besides as-purchased and PVP/ethanol treated membranes as control. Based on the experimental conditions employed, the effective ion conductivity and thus diffusion coefficient (D_{ion}^{mem}) *albeit* indirect corresponding to ion flux through the nanopores of the bioinspired membranes that are related to the evolution of ionic conductivity measured. Qualitatively, it is apparent that the ion conductivity is higher for those membranes impregnated with artificial biological ion channel proteins and equivalent with GO conjugation where the proteins were confined than those of untreated and unfunctionalized membranes.

Preprints (www.preprints.org) | NOT PEER-REVIEWED | Posted: 26 April 2023 doi:10.20944/preprints202304.0977.v1

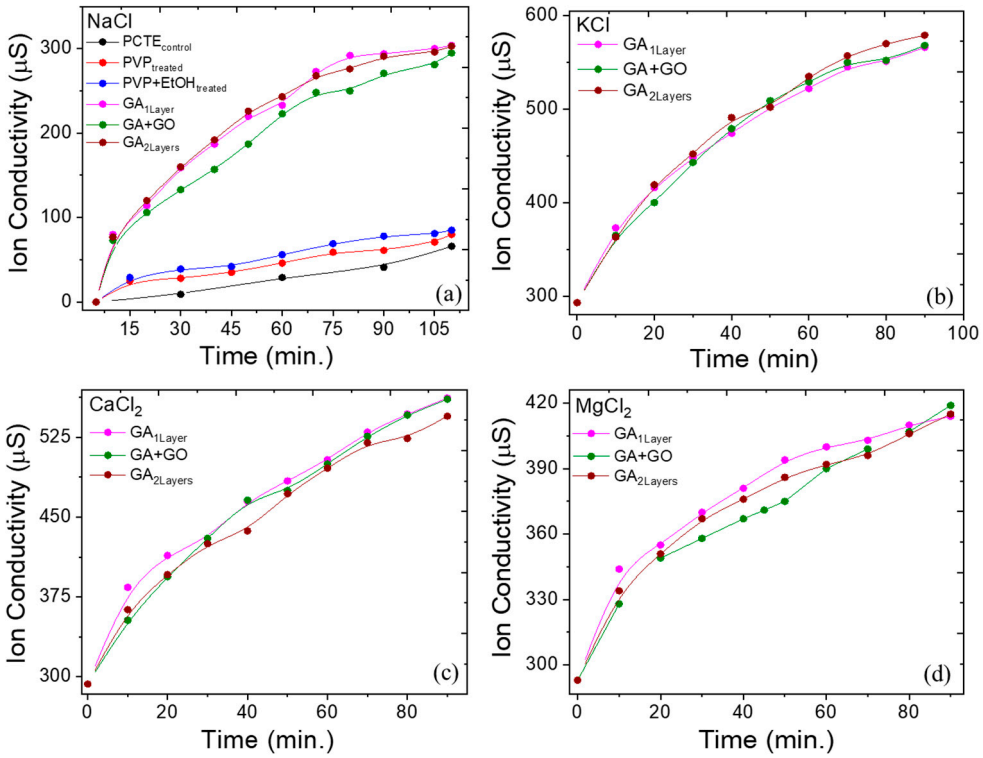

Figure 3. Membrane performance through ion diffusion. (a–d) Representative ion conductivity variation with time for NaCl, KCl, $CaCl_2$, and $MgCl_2$ for PCTE-based membranes (approach1) with GA and GA+GO along with control.

Quantitatively, the ion diffusion and permeability increased significantly by two to three orders of magnitude for GA and GA+GO treated membranes from untreated and PVP+EtOH treated PCTE membranes as apparent from Figure 4a,b. We also determined the relative ion permeability P_{ion}^{rel} shown in Figure 4b which is enhanced by almost three to four orders of magnitude. The Figure 4c summarizes the ratio of D_{ion}^{mem} divided by self-diffusion coefficient of cation in bulk water D_{ion}^{bulk} for the membranes studied. The ratio of $D_{ion}^{mem}/D_{ion}^{bulk}$ value which is between 3–5 for the untreated membranes increased to around 13-16 for GA, α-HL, and OmpF impregnated membranes. However, the ratio is somewhat independent of either the protein ion channel type, the chloride solution, or concentration. Lastly, no significant ion selectivity is observed between the mono- and divalent cations except for α-HL which showed marginal selectivity over Na^+ and Ni^{2+} ions. Other inferences that can be drawn from the experimental observations are: (i) First, the ratio obtained for GA-free membranes is slightly higher pointing out that the nanopores contribute themselves to an increase of ion diffusion attributed to effective surface charge density. This effect becomes significant for lower concentration due to increase of Debye length. This finding agrees with experiments for alkali ion and chlorine ion diffusion in nanopores and with models based on size exclusion effect [13,14] (ii) second, when ethanol-treated membrane is impregnated with GA, ion diffusion recovers from the level measured for the non-impregnated membrane. The primary interpretation of this outcome is that GA strongly influences the effective ion diffusion when there is a critical loading of proteins inside the nanopores. The experimental values of diffusion coefficient also implies that proteins do not impede the ion diffusion. Thus, we can decisively claim that ions diffuse through the proteins confined nanopores yet without direct interaction. It is consistent with the presumption that proteins neither improve nor obstruct membrane permeability. Though we have no means to evaluate the origin of D_{ion}^{mem} increase since presence of proteins inside the nanopore modify either the intrinsic ion diffusion due to specific action on mobility or concentration due to its electrostatic interaction and hence exclusion-enrichment effect (EEE) [63]. One of the easiest ways to discriminate between these effects would be to measure ion concentration inside the nanopore which is quite challenging

Preprints (www.preprints.org) | NOT PEER-REVIEWED | Posted: 26 April 2023 doi:10.20944/preprints202304.0977.v1

because of extremely small volume of nanopore compared to compartment (1) electrolyte in diffusion cell. The other approaches could involve solving the Poisson-Boltzmann equation for protein-nanopore system. Additionally, the confinement and conformation of these artificial ion channels forming proteins of nanoscale dimension within the support membrane hydrophobic surface needs to be elucidated. While confocal fluorescence microscopy/spectroscopy was used experimentally [49,64], unconstrained molecular dynamics (MD) simulations is also a powerful tool for deeper insights about the relationship between the structural features of confined proteins and associated functionality (ion permeability and diffusion) [49]. However, it is admissible that they require precise description simulating the system which is beyond the scope of this study.

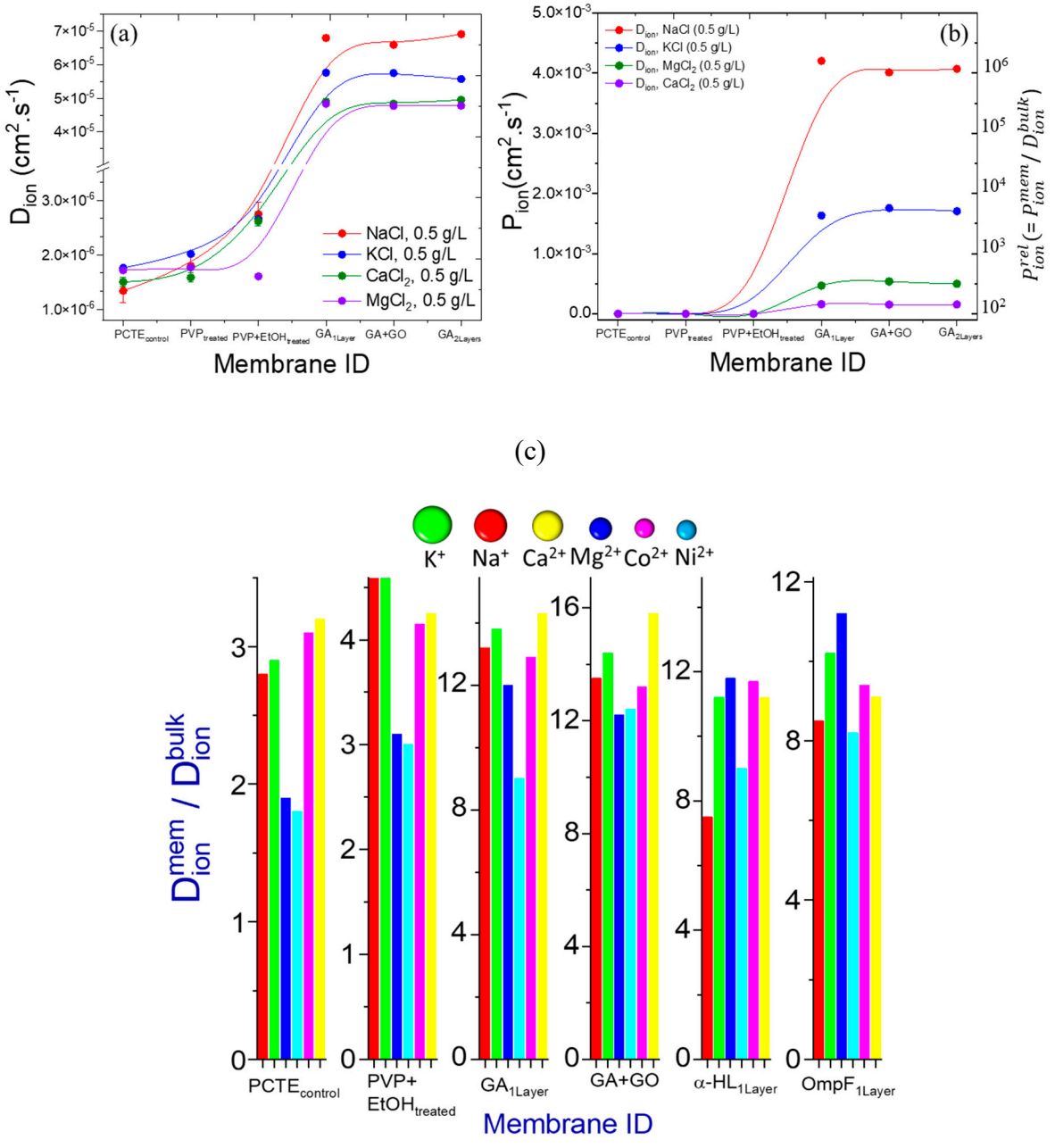

Figure 4. Permeation tests and properties. (a) Ion diffusion coefficient, D_{ion} (b) ion permeability, P_{ion}, and relative ion permeability, P_{ion}^{rel} (ratio of permeability through membrane to bulk ion diffusivity=$P_{ion}^{mem}/D_{ion}^{bulk}$). (c) Histogram of the ratio between ion diffusion coefficient through the membrane nanopores D_{ion}^{mem} and D_{ion}^{bulk} for various electrolyte ions.

Preprints (www.preprints.org) | NOT PEER-REVIEWED | Posted: 26 April 2023 doi:10.20944/preprints202304.0977.v1

The relatively higher retention (R, rejection of unwanted ions) and higher adsorption (Ads.) percentage of monovalent (Na^+, K^+) and divalent (Ca^{2+}) ions as compared with Mg^{2+} imply that the protein accommodation inside the nanopores point at not so favorable orientation of GA protein ion channel (Figure 5a,b). While observing the variation of D_{ion} for all these electrolytes (Figure 4c), it is also apparent that monovalent (Na^+, K^+) and divalent (Ca^{2+}) ions as compared with Mg^{2+} and Ni^{2+} are higher, which indicates the lack of selectivity. Thus, these experimental results help us to explain that GA is either double stranded dimer or stable β-helical conformation and why the confined GA (and other ion channel proteins tested in this study) did not exhibit selectivity. Alternatively, the higher ion diffusion coefficient for three ions from confined GA protein indicates that they diffuse selectively these ions compared with Mg^{2+} ions. Interestingly, the relative permeability $P_{ion}^{rel} = D_{ion} \times K$, which is proportional to ion diffusivity weighted with solubility coefficient or partition coefficient, is higher for $CaCl_2$ (Figure 4c) than those of other ions supporting minimum surface adsorption. The salt ion rejection is an important factor for effectiveness of membranes besides principle of confinement in nanopores for describing the performance of bioinspired nanoporous membranes. The narrow pore size is a barrier to ions, however, with shorter pore-pore distance allows for smaller transport barrier. Based on the ion diffusion measurements, it is established that GA and other proteins were confined into the cylindrical nanopores, and it enhances the ion conductance and relative permeability. Although the bio-membranes studied in this work did not exhibit outstanding ion selectivity, it opens a promising field of research in the domain of nano-biofiltration based on differential ion conduction.

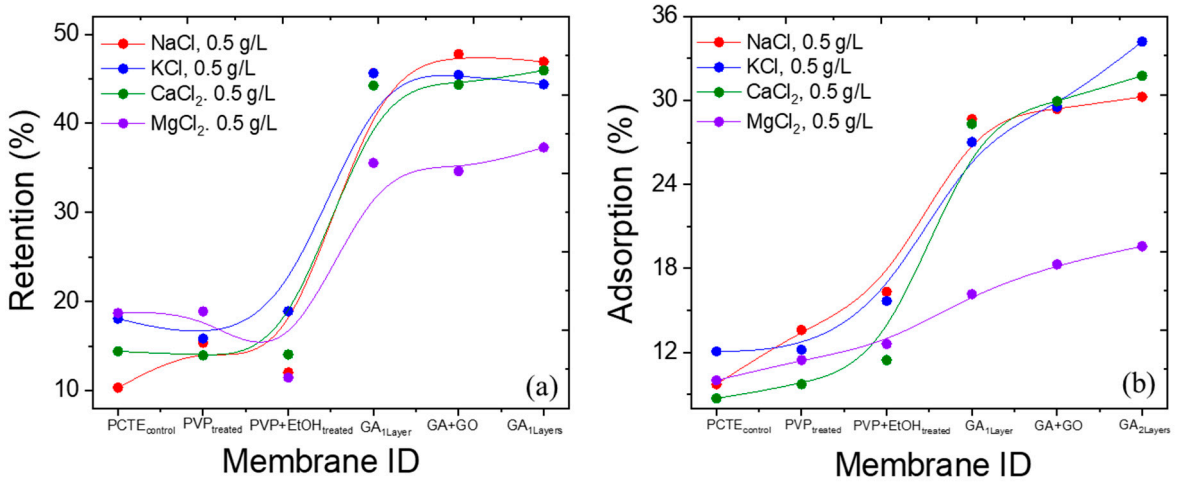

Figure 5. PCTE-based membranes performance using dead-end filtration for NaCl, KCl, $CaCl_2$, and $MgCl_2$ with GA_{1Layer}, GA+GO and $GA_{2Layers}$ along with control: (a) Retention and (b) Adsorption percentage.

3.3. Ion transport through GO conjugated ion recognition peptides membranes

For this approach 2, we synthesized functionalized graphene oxide (GO-COOH) and conjugated with selective ion recognition short chain peptides having specific sequence with strong affinity for transition metal cobalt and nickel cations. Peptide1 (Co_{pep}) that has a strong binding affinity for cobalt ions (Co^{2+}), is compared with the peptide2 (Na_{pep}) and a random chain peptide3 (RF_8). We used mixed cellulose ester (MCE) support membrane and evaluated their performance besides control. The ion recognition capability of peptide motifs for Co^{2+} identified in a bioplanning method translates into bioinspired ion selective filters, while for other ions it is not known. For further comparisons, we tested them with membranes functionalized with proteins2 (α-HL) and protein3 (OmpF). Figure 6a-6e shows time evolution ion conductance in compartment (2) for KCl and $MgCl_2$ of 0.5 g/L and $NiCl_2$ and $CoCl_2$ of 0.1M concentrations besides MCE control. The diffusion for Co^{2+} ion was the strongest with GO-Co_{pep} followed by Ni^{2+} ion being the highest with GO-Na_{pep} peptide. Interestingly, the ion diffusion for KCl and $MgCl_2$ was smaller for all the peptides and proteins. All the membrane

Preprints (www.preprints.org) | NOT PEER-REVIEWED | Posted: 26 April 2023 doi:10.20944/preprints202304.0977.v1

performance was evaluated for 1.5–2 h after soaking them for 10–12 h to the corresponding aqueous salt solutions and we did not observe visible salt adsorption on the surface of membranes. More importantly, only a marginal difference in conductance values was found between different transition metal ions. We postulate that the recognition of target Co^{2+} ions facilitated by the transport of ions where recognition elements locate when the dissociation constant between peptides and the ions is not too small. If the binding with targets is stronger, the functional molecules will capture targets blocking the transport through channel such as in the case of K^+ and Mg^{2+} ions for all the membranes investigated. In analogy with the approach 1, we quantified the performance of these membranes in terms of ion diffusion coefficient, permeability and relative ion permeability summarized in Figure 6f,g, respectively. The ion permeability was calculated through the membranes from the slope of a concentration-time curve. While these results do not signify the selectivity between transition metal ions, the results showed strong differences for alkali and alkaline metal ions. Also, the adsorption tests do not necessarily reflect the ion selectivity of peptide1 and peptide2 based membranes towards Co^{2+} and Ni^{2+} originated from adsorption efficiency of GO-Co_{pep} and GO-Na_{pep}, respectively. We believe that the preferential affinity of Co_{pep} and Na_{pep} towards Co^{2+} and Ni^{2+} compared with K^+ and Mg^{2+} significantly contributes to ion selectivity. Alternatively, the binding of transition metal ions may not be too strong to be captured or trapped but favorable enough to induce preferential interaction for selective ion transport. To be noted is the relative permeability which is sufficiently high enough for Co^{2+} ion followed by Ni^{2+} and the much lower for K^+ and Mg^{2+} ions showing once again the selectivity towards transition metal ions.

To complement the ion conductivity measurements, UV-vis spectroscopy was carried out to monitor and to determine the concentration on the pure side of water compartment 2 for 90–120 min. Figure 7 shows the representative time evolution of absorption (Figure 7a–c,f,g) and fluorescence (Figure 7d,e) spectra for peptide1, peptide2, protein2, and protein3 with Co^{2+} and Ni^{2+} ions. The ion permeability can be calculated from the slope of concentration-time curves shown in Figure 7h,i. The relative permeability defined though diffusion and solubility coefficient of Co^{2+}, Ni^{2+}, Mg^{2+} and K^+ ions through bare MCE and GO conjugated membranes with both peptides and proteins summarized in Figure 6g. The degree of ion transport enhancement is defined as the relative permeability of a specific ion as the ratio of membrane permeability over bulk diffusivity. The faster transport reported for GO membranes has been attributed to its inherent physical-chemical property briefly described below [14,20,41]. However, this study focuses on the ion selectivity which is obtained from the ratio of relative permeability of Co^{2+} ion to that of ions under comparison. In Figure 8a, GO-COOH showed no sizeable selectivity for Co^{2+} over Ni^{2+} and Mg^{2+} ions. The selectivity of ~3 to 4 was attained for Co^{2+} over Ni^{2+} ion for peptide1 and peptide2, respectively as summarized in Figure 8a-8b. Interestingly, Co_{pep} (peptide1) did not show clear selectivity for Co^{2+} over Ni^{2+} ion. The selectivity through artificial ion channel filters between ions of similar properties (transition metal cations) was about 3. Thus, the ion selectivity was marginally higher for GO-Co_{pep} membranes than those of reported previously from solid state ion channels [65,66]. The selectivity was also tested with GO-RF8 (peptide3) as negative control, mimicking the water selective filter in aquaporin, which showed no selectivity for Mg^{2+} and Ni^{2+} ion over Co^{2+} (Figure 8c) which implies it is rooted in unique functionality of Co_{pep} molecules. Notably, the selectivity over Mg^{2+} and Ni^{2+} ion is many times, which is almost twice than previously reported values for selectivity between cations. The same peptides functionalized on the larger nanochannels have somewhat lower selectivity and it turns out selectivity for nano-channels larger than 6 nm completely. It is suggested the novel platform with desirable dimension is indispensable for mimicking biological attributes to natural ion channels.

Preprints (www.preprints.org) | NOT PEER-REVIEWED | Posted: 26 April 2023 doi:10.20944/preprints202304.0977.v1

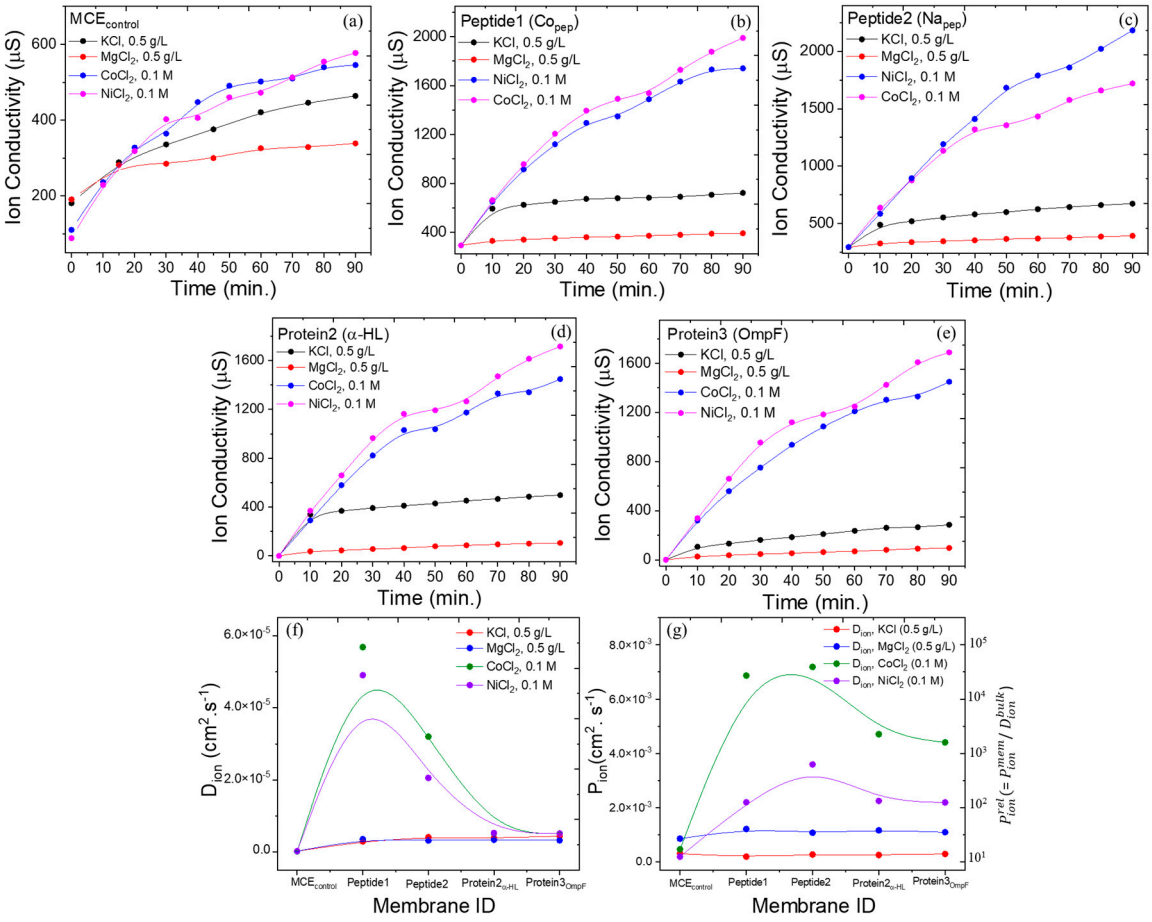

Figure 6. MCE-based membranes performance using ion diffusion cell. Ion conductivity variation of KCl, $MgCl_2$, $CoCl_2$, and $NiCl_2$ with (a) MCE control (b) Co_{pep} (peptide1) (c) Na_{pep} (peptide2), (d) α–HL (protein2), and (e) OmpF (protein3) conjugated with GO (f) Ion diffusion coefficient, D_{ion} (g) ion permeability P_{ion}, and relative ion permeability P_{ion}^{rel}.

Preprints (www.preprints.org) | NOT PEER-REVIEWED | Posted: 26 April 2023 doi:10.20944/preprints202304.0977.v1

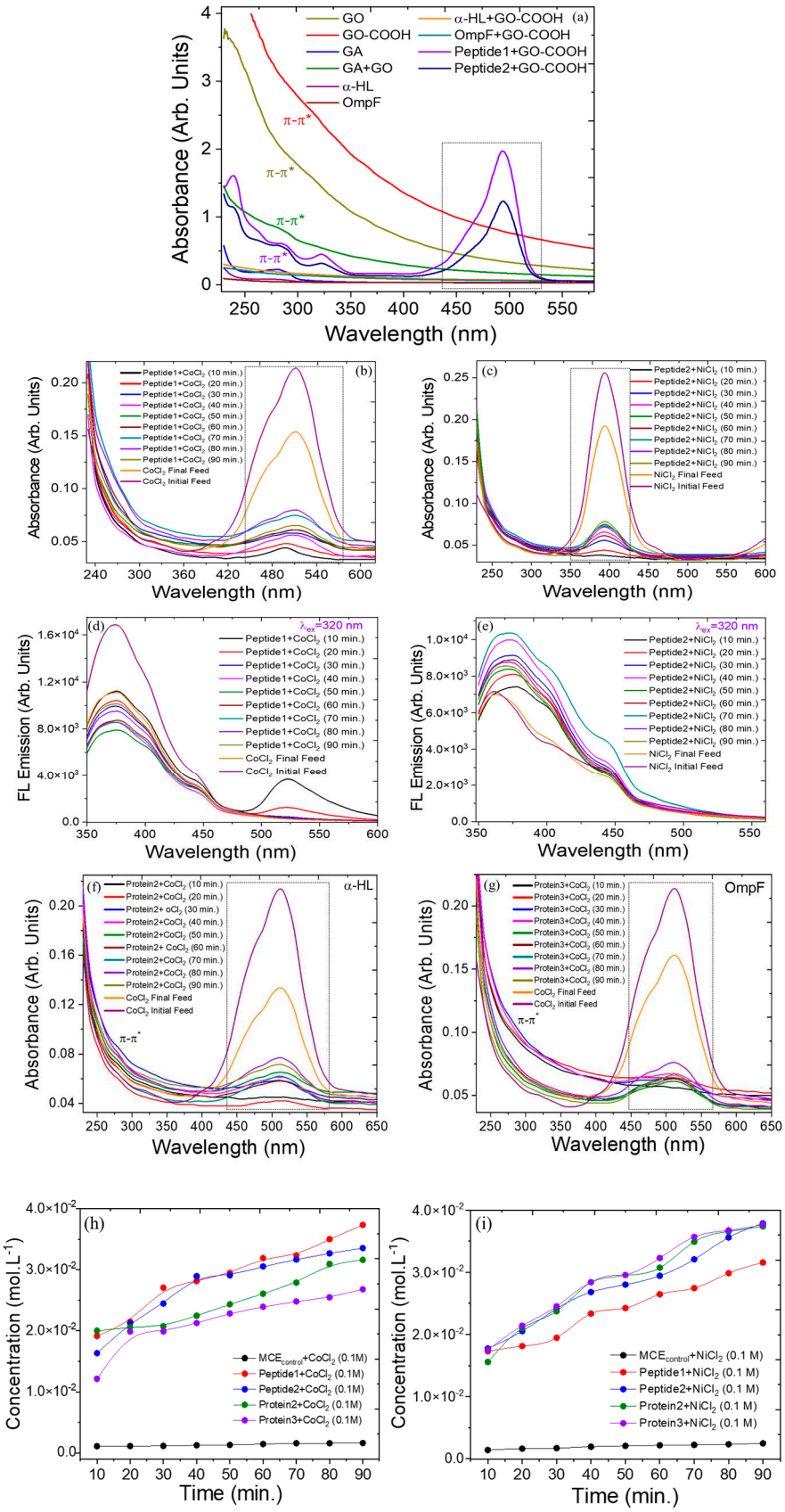

Figure 7. (a) UV-Visible absorption spectra of various components. Time evolution (b, c) absorption and (d, e) fluorescence spectra of Co^{2+} and Ni^{2+} ions transported through peptide 1 and peptide 2 along with (f, g) protein1 and protein2. (h, i) Quantitative determination of (h) Co^{2+} and (i) Ni^{2+} ion concentration from absorption spectra.

Preprints (www.preprints.org) | NOT PEER-REVIEWED | Posted: 26 April 2023 doi:10.20944/preprints202304.0977.v1

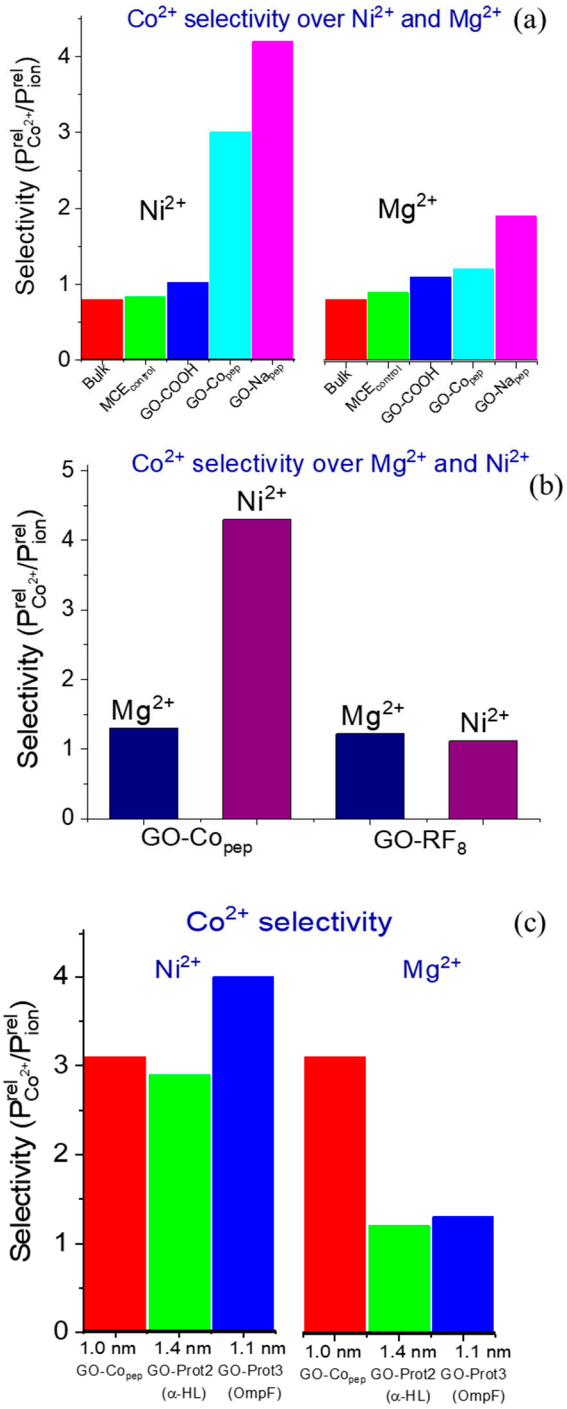

Figure 8. (a) Selectivity of Co^{2+} ion over Ni^{2+} and Mg^{2+} ions depending on the surface and peptides 1 and 2. (b) Selectivity of Co^{2+} ion over Mg^{2+} over Ni^{2+} ions depending on peptide 1 and random peptide ($GO\text{-}RF_8$). (c) Effect of nanochannel diameter on Co^{2+} ion selectivity over Ni^{2+} and Mg^{2+} from peptide1 ($GO\text{-}Co_{pep}$), protein2 (α–HL), and protein3 (OmpF).

In biology, ion specificity of the transporters is endowed by the specific metal ion binding affinity to the residue or amino acid sequence in the peptide motifs or protein structure [27,28]. The coordination chemistry of metal ion-peptides is fundamental to biological discrimination. For instance, Ni^{2+} and Zn^{2+} ions prefer sulfur ligands, hence they bind to histidine (His, H), and cysteine (Cys, C) based on acid-base theory [67]. Co_{pep} with EPGHDAVP sequence has histidine residue and

Preprints (www.preprints.org) | NOT PEER-REVIEWED | Posted: 26 April 2023 doi:10.20944/preprints202304.0977.v1

acidic residue (glutamate E and aspartate D) as in most Co^{2+} ion binding motifs. Likewise, Na_{pep} also has acidic residue (glutamate E and aspartate D) which also shows affinity for Ni^{2+} ion. Apart from coordination chemistry, geometric components also constitute the recognition. The coordination geometry is also closely related to the d-block electronic configuration of transition metal. This study demonstrates encouraging results for selective ion transport by using biomimetic recognition chemistry and synergistic combination of such chemistry with novel nanomaterials like GO or GO-COOH providing variable hydrophilicity as compared to pristine membranes, potentially reducing internal electrolyte concentration polarization. Therefore, the addition of a small amount of nanomaterial significantly improves the physicochemical properties of membranes. In particular, the carbons in GO nanosheets contain aromatic regions with unoxidized benzene rings and aliphatic regions with six-membered carbon rings and lateral domains size depends on the degree of oxidation.[Error! Bookmark not defined.] In the size exclusion model, the rejection of ionic species is controlled by the charge density of the membrane following [68]:

$$R = 1 - \frac{C_p}{C_f} = 1 - \left(\frac{|Z_i|C_f}{|Z_i|C_p + X}\right)^{\left|\frac{z_i}{z_j}\right|} - (6),$$

where C_f and C_p are concentration (ionic conductivity in this study) in the feed and permeate solutions, X is the membrane charge density, i and j subscripts refer to co- and counter-ions and Z the ion valency. Computer simulations show that graphene containing oxygenated groups lined nanopores/nanochannels, can trap K^+ and Mg^{2+} ions under certain electrochemical conditions. Additionally, it was established from proton exchange membranes (PEM) in fuel cells to ion channels in biological membranes, that the well-specified control of ionic interactions in confined geometries influences the ion transport and selectivity profoundly.

4. Conclusions

We explored the feasibility of producing large-area membranes integrating artificial protein ion channels within a network of relatively aligned nanpores in support membranes and graphene oxide conjugated bioinspired peptides having specific sequence working as ion selective filters. Biomimetic approaches are germane to bioinspired functional molecules imitating the function and principle of biological ion channels. Specifically, we reported the design and development of scalable nanoporous membranes from (1) solid-state polymer track etched support in which ion channels were confined (bioinspired; approach1) and (2) mixed cellulose ester network modified with GO conjugated short chain peptide motifs for ion selectivity (biomimetic; approach2). Ion recognition capability of the chosen peptide motifs translated into ion specificity for diffusive transport. The experimental measurements demonstrated that the ion channel proteins are confined within the nanopores, resulting in the enhancement of ionic permeability and diffusion. For the second approach, peptide motifs as ion transporters had the capabilities for selective ion recognition via binding affinity towards transition metal ion. We emphasize the importance of bio-functionalization on solid support which allows controlled ion transport as in biological ion channels and capable to sustain mechanical stress during fabrication and monitoring diffusion kinetics with stirring, both attributed to the good mechanical properties of GO nanosheets. These novel approaches enabled by nanotechnology open new avenues for developing artificial ion channels via synergistic combination of biomimetic recognition surface chemistry and functionalized graphene platforms. Fabricating membranes with nanochannels through these approaches are applicable to other two-dimensional layered materials such as MoS_2 nanolayers and a suite of peptide motifs for specific metal ions via bioplanning method. The latter can provide enormous potential for accelerated discovery and innovations in the field of water nanofiltration, purification and desalination via ion selectivity and molecular separation.

Author Contributions: S. Gupta: Conceptualization, Investigation, Data curation, Analysis, Supervision, Funding acquisition, Resources, Writing - original draft, Reviewing and Editing. **T. Robinson:** Data curation, Analysis. **B. Evans:** Data curation, Analysis.

Data Availability: The data that support the findings of this study are available within the article.

Acknowledgments: The author (S.G.) gratefully acknowledges financial support by NSF-MRI (Grant# 1429563), KY NSF EPSCoR RSP (subaward# 3200000271-17-212) and co-author (T.R.) for researcher scholarship, and internal RCAP WKU Foundation award. The undergraduate student co-authors (T.R., B.E.) are grateful to John Andersland (Biology) and Naomi Rowland (Biology) for scanning electron microscopy and confocal fluorescence spectroscopy training, respectively.

Declaration of Competing Interest: The authors declare that they have no known competing financial interests that could have appeared to influence the work reported in this paper.

References

[1]. C. A. Grady, S.-C. Weng, E. R. Blatchley III, in Potable Water, Springer, pp. 37–59 (2014).

[2]. R. Jain, Providing safe drinking water: a challenge for humanity, Clean Technol. Environ. Policy, 14 (2012) 1-9.

[3]. M. A. Shannon, P. W. Bohn, M. Elimelech, J. G. Georgiadis, B. J. Marinas, A. M. Mayes, Science and technology for water purification in the coming decades, Nature 452 (2008) 301–310.

[4]. *https://www.nsf.gov/pubs/2018/nsf18545/nsf18545.htm*

[5]. D. L. Shaffer, N. Y. Yip, J. Gilron, M. Elimelech, Seawater desalination for agriculture by integrated forward and reverse osmosis: Improved product water quality for potentially less energy, J. Memb. Sci. 415 (2012) 1-8.

[6]. L. Huang, M. Zhang, C. Li, G. Shi, Graphene-based membranes for molecular separation, J. Phys. Chem. Lett. 6 (2015) 2806–2815.

[7]. M. Hu, B. Mi, Enabling graphene oxide nanosheets as water separation membranes, Environ. Sci Technol. 47 (2013) 3715-3723.

[8]. M. Elimelech, The global challenge for adequate and safe water, J. Water Supply Res. Technol.- AQUA 55 (2006) 3-10.

[9]. F. Perreault, A. F. de Faria, M. Elimelech, Environmental applications of graphene-based nanomaterials, Chem. Soc. Rev. 44 (2015) 5861–5896.

[10]. D. Chohen-Tanugi, J. C. Grossman, Mechanical Strength of Nanoporous Graphene as a Desalination Membrane, Nano Lett. 14 (2014) 6171–6178.

[11]. L. F. Greenlee, D.F. Lawler, B.D. Freeman, B. Marrot, P. Moulin, Reverse osmosis desalination: water sources, technology, and today's challenges, Water Res. 43 (2009) 2317–2348.

[12]. T. Basile, A. Petrella, M. Petrella, G. Boghetich, V. Petruzzelli, S. Colasuonno, D. Petruzzelli, Review of endocrine-disrupting-compound removal technologies in water and wastewater treatment plants: An EU perspective, Ind. Eng. Chem. Res. 50 (2011) 8389-8401.

[13]. M. Buonomenna, Nano-enhanced reverse osmosis membranes, Desalination, 314 (2013) 73-80.

[14]. S. Gupta, A. Henson, B. Evans, Novel formulations for scalable multilayer nanoporous graphene-based membranes for use in efficient water detoxification revisited, Desalination and Water Treatment, 169 (2019) 59–71.

[15]. S. Garaj, S. Liu, J. A. Golovchenko, D. Branton, Molecule-hugging graphene nanopores, Proc. Nat. Acad. Sci. 110 (2013) 12192-12196.

[16]. M. Elimelech, The global challenge for adequate and safe water, J. Water Supply: Res. Technol.-AQUA 55 (2006) 3-10.

[17]. M. M. Pendergast, E. M. V. Hoek, A review of water treatment membrane nanotechnologies, Energy Environ. Sci. 4 (2011) 1946-1971.

[18]. S. Gupta, B. Evans, Interplay of graphene oxide and interfacial polymerized polyamide-crosslinked thin-film composite membranes for enhanced performance during reverse osmosis, Desalination and Water Treatment, 218 (2021) 177–192.

[19]. G. M. Geise, H. S. Lee, D. J. Miller, B. D. Freeman, J. E. Mcgrath, D. R. Paul, Water purification by membranes: the role of polymer science, J. Polym. Sci. Part B: Polym. Phys. 48 (2010) 1685-1718.

[20]. C.R. Martin, M. Nishizawa, K. Jirage, M.S. Kang, S.B. Lee, Controlling ion–transport selectivity in gold nanotubule membranes, Adv. Mater. 13 (2001) 1351−1362.

[21]. M. Ali, B. Yameen, R. Neumann, W. Ensinger, W. Knoll, O.J. Azzaroni, Biosensing and Supramolecular Bioconjugation in Single Conical Polymer Nanochannels. Facile Incorporation of Biorecognition Elements into Nanoconfined Geometries, Am. Chem. Soc. 130 (2008) 16351−16357.

[22]. I. Vlassiouk, T.R. Kozel, Z.S. Siwy, Biosensing with Nanofluidic Diodes, J. Am. Chem. Soc. 131 (2009) 8211−8220.

[23]. S. Majd, E.C. Yusko, Y.N. Billeh, M.X. Macrae, J. Yang, M. Mayer, Applications of biological pores in nanomedicine, sensing, and nanoelectronics, Curr. Opin. Biotechnol. 21 (2010) 439−476.

[24]. B.E. Logan, M. Elimelech, Membrane-based processes for sustainable power generation using water, Nature, 488 (2012) 313−319.

[25]. J. Zhao, X. Zhao, Z. Jiang, Z. Li, X. Fan, J. Zhu, H. Wu, Y. Su, D. Yang, F. Pan, J. Shi, Biomimetic and bioinspired membranes: Preparation and application, Prog. In Polym. Sci. 39 (2014) 1668-1720.

[26]. S. P Tsunoda, B. Wiesner, D. Lorenz, W. Rosenthal, P. Pohl, Aquaporin-1, nothing but a water channel, J. Biol. Chem. 279 (2004) 11364-11367.

[27]. B. Hille, in *Ion Channels of Excitable Membranes*, 3rd Ed.; Sinauer Associates: Sunderland, MA (2001).

[28]. S. Gupta, J. Dura, A. Freites, D. Tobias, J. K. Blasie, Structural characterization of the voltage sensor domain and voltage-gated K^+-channel proteins vectorially oriented within a single bilayer at the solid/vapor and solid/liquid interfaces via neutron interferometry, Langmuir 28 (2012) 10504-10520; *S. Gupta, J. Dura, A. Freites, D. Tobias and J. K. Blasie, Featured at NIST-NCNR Headline News, One of 20 most cited article in the field of Ion Channel Protein Biophysics (BioMedLib)*

[29]. A. Tronin, C.-H. Chen, S. Gupta, D. Worcester, V. Lauter, J. Strzalka, I. Kuzmenko and J.K. Blasie, Structural changes in single phospholipid membranes in response to an applied transmembrane electric potential revealed by time-resolved neutron/X-ray interferometry, Chemical Physics, 422 (2013) 283-289 (Invited).

[30]. S. Gupta, J. Liu, J. Strzalka, J. K. Blasie, Profile structure of the voltage sensor domain and KvAP channel within single membranes *via* X-ray interferometry, Phys. Rev. E 84 (2011) 031911-1-15.

[31]. K. Ariga, Silica-supported biomimetic membranes, Chem. Rec. 4 (2004) 59–59.

[32]. W. Meier, C. Nardin, M. Winterhalter, Reconstitution of Channel Proteins in (Polymerized) ABA Triblock Copolymer Membranes, Angew. Chem. Int. Ed. 39 (2000) 4599.

[33]. M. Kumar, M. Grzelakowski, J. Zilles, M. Clark, W. Meier, Highly permeable polymeric membranes based on the incorporation of the functional water channel protein Aquaporin Z, Proc. Natl. Acad. Sci. U.S.A. 104 (2007) 20719–20724.

[34]. A. Gonzalez-Perez, K.B. Stibius, T. Vissing, C.H. Nielsen, O.G. Mouritsen, Biomimetic Triblock Copolymer Membrane Arrays: A Stable Template for Functional Membrane Proteins, Langmuir 25 (2009) 10447–10450.

[35]. C. Dekker, Solid-state nanopores, Nat. Nanotechnol. 2 (2007) 209–215.

[36]. M. Ali, S. Nasir, Q.H. Nguyen, J.K. Sahoo, M.N. Tahir, W. Tremel, W. Ensinger, Metal ion affinity-based biomolecular recognition and conjugation inside synthetic polymer nanopores modified with iron–terpyridine complexes, J. Am. Chem. Soc. 133 (2011) 17307−17314.

[37]. S. P. Surwade, S. N. Smirnov, I. V. Vlassiouk, R. R. Unocic, G. M. Veith, S. Dai, S. M. Mahurin, Water desalination using nanoporous single-layer graphene, Nat. Nanotechnol. 10 (2015) 459–464.

[38]. M. L.-Hidalgo, S. Hu, O. Marshall, A. Mishchenko, A. N. Grigorenko, R. A. W. Dryfe, B. Radha, I. V. Grigorieva, A. K. Geim, Sieving hydrogen isotopes through two-dimensional crystals, Science 351 (2016) 68–70.

[39]. R. K. Joshi, P. Carbone, F. C. Wang, V. G. Kravets, Y. Su, I. V. Grigoriev1, H. A. Wu, A. K. Geim, R. R. Nair, Precise and ultrafast molecular sieving through graphene oxide membranes, Science 343 (2014) 752–754.

[40]. D. Konatham, J. Yu, T. A. Ho, A. Striolo, Simulation insights for graphene-based desalination membranes, Langmuir 29 (2013) 11884–11897.

[41]. H.B. Wang, Q. Zhang, X. Chu, T.T. Chen, J. Ge, R.Q. Yu, Graphene oxide-peptide conjugate as an intracellular protease sensor for caspase-3 activation imaging in live cells, Angew. Chem. Int. Ed. 50 (2011) 7065–7069.

[42]. L.M. Zhang, J.G. Xia, Q.H. Zhao, L.W. Liu, Z.J. Zhang, Functional graphene oxide as a nanocarrier for controlled loading and targeted delivery of mixed anticancer drugs, Small, 6 (2010) 537–544.

[43]. P. Sun, M. Zhu, K. Wang, M. Zhong, J. Wei, D. Wu, Z. Xu, H. Zhu, Selective Ion Penetration of Graphene Oxide Membranes, ACS Nano, 7 (2012) 428-436.

[44]. A. Calvo, B. Yameen, F.J. Williams, G. Soler-Illia, O. Azzaroni, Mesoporous Films and Polymer Brushes Helping Each Other To Modulate Ionic Transport in Nanoconfined Environments. An Interesting Example of Synergism in Functional Hybrid Assemblies, J. Am. Chem. Soc. 131 (2009) 10866–10868.

[45]. H. W. Kim, H.W. Yoon, S.M. Yoon, B.M. Yoo, B.K. Ahn, Y.H. Cho, H.J. Shin, H. Yang, U. Paik, S. Kwon, J.Y. Choi, H.B. Park, Selective gas transport through few-layered graphene and graphene oxide membranes, Science, 342 (2013) 91–95.

[46]. A. Cazacu, Y.M. Legrand, A. Pasc, G. Nasr, A. Van der Lee, E. Mahon, M. Barboiu, Dynamic hybrid materials for constitutional self-instructed membranes, Proc. Natl. Acad. Sci. U. S. A. 106 (2009) 8117–8122.

[47]. P. Kohli, C.C. Harrell, Z. H. Cao, R. Gasparac, W.H. Tan, C.R. Martin, DNA–nanotube artificial ion channels, Science 305 (2004) 984–986.

[48]. S. Kim, J. Nham, Y. S. Jeong, C. S. Lee, S. H. Ha, H. B. Park, Y. J. Lee, Biomimetic selective ion transport through graphene oxide membranes functionalized with ion recognizing peptides, Chem. Mater. 27 (2015) 1255-1261.

[49]. S. Balme, J.-M. Janot, L. Berardo, F. Henn, D. Bonherry, S. Kraszewski, F. Picaud, and C. Ramseyer, New bioinspired membrane made of a biological ion channel confined into the cylindrical nanopore of a solid-state polymer, Nano Lett. 11 (2011)712-716.

[50]. W. Guo, L.X. Cao, J.C. Xia, F.Q. Nie, W. Ma, J.M. Xue, Y.L. Song, D.B. Zhu, Y.G. Wang, L. Jiang, Energy Harvesting with Single-Ion-Selective Nanopores: A Concentration-Gradient-Driven Nanofluidic Power Source, Adv. Funct. Mater. 20 (2010) 1339–1344.

[51]. http://www.uniprot.org/

[52]. K.M. Williams, E.C. Bigley, 3rd, R. B. Raybourne, Identification of murine B-cell and T-cell epitopes of *Escherichia coli* outer membrane protein F with synthetic polypeptides, Infect Immun. 68 (2000) 2535–2545.

[53]. M. Sarikaya, C. Tamerler, A. K. Y. Jen, K. Schulten, F. Baneyx, Molecular biomimetics: nanotechnology through biology, Nat. Mater. 2 (2003) 577−585.

[54]. U. Hersel, C. Dahmen, H. Kessler, RGD modified polymers: biomaterials for stimulated cell adhesion and beyond, Biomaterials, 24 (2003) 4385−4415.

[55]. C. L. Chen, N.L. Rosi, Peptide-Based Methods for the Preparation of Nanostructured Inorganic Materials, Angew. Chem. Int. Ed. 49 (2010) 1924−1942.

[56]. S. R. Whaley, D.S. English, E. L. Hu, P.F. Barbara, A.M. Belcher, Selection of peptides with semiconductor binding specificity for directed nanocrystal assembly, Nature, 405 (2000) 665−668.

[57]. D.Y. Oh, X. N. Dang, H.J. Yi, M.A. Allen, K. Xu, Y.J. Lee, A.M. Belcher, Graphene Sheets Stabilized on Genetically Engineered M13 Viral Templates as Conducting Frameworks for Hybrid Energy-Storage Materials, Small, 8 (2012) 1006−1011.

[58]. B. He, G. Chai, Y. Duan, Z. Yan, L. Qiu, H. Zhang, Z. Liu, Q. He, K. Han, B. Ru, F.-B. Guo, H. Ding, H. Lin, X. Wang, N. Rao, P. Zhou, J. Huang, BDB: biopanning data bank, Nucleic Acids Res. 44 (2016) D1127−D1132.

[59]. S. K. Lee, D.S. Yun, A.M. Belcher, Cobalt ion mediated self-assembly of genetically engineered bacteriophage for biomimetic Co−Pt hybrid material, Biomacromolecules, 7 (2006) 14−17.

[60]. P. W. Atkins, in *Physical Chemistry*, 5th Ed. Oxford University Press (1992).

[61]. S. P. Pinho and E. A. Macedo, Solubility of NaCl, NaBr, and KCl in Water, Methanol, Ethanol, and Their Mixed Solvents, J. Chem. Eng. Data 50 (2005) 29-32.

[62]. S. Balme, J.M. Janot, P. Dejardin, E.N. Vasina, P. Seta, Potentialities of confocal fluorescence for investigating protein adsorption on mica and in ultrafiltration membranes, J. Memb. Sci. 284 (2006) 198–204.

[63]. A. Plecis, R.B. Schoch, P. Renaud, Ionic Transport Phenomena in Nanofluidics: Experimental and Theoretical Study of the Exclusion-Enrichment Effect on a Chip, Nano Lett. 5 (2005) 1147–1155.

[64]. S. Balme, J. M. Janot, P. Dejardin, E.N. Vasina, P. Seta, Potentialities of confocal fluorescence for investigating protein adsorption on mica and in ultrafiltration membranes, J. Memb. Sci. 284 (2006) 198–204.

[65]. M. Barboiu, Y. Le Duc, A. Gilles, P.A. Cazade, M. Michau, Y.M. Legrand, A. *van der* Lee, B. Coasne, P. Parvizi, J. Post, T. Fyles, An artificial primitive mimic of the Gramicidin-A channel, Nat. Commun. 5 (2014) 4142−4146.

 doi:10.20944/preprints202304.0977.v1

[66]. C. Dekker, Solid-state nanopores, Nat. Nanotechnol. 2 (2007) 209–215.

[67]. X.S. Sun, C.L. Xiao, R.G. Ge, X.F. Yin, H. Li, N. Li, X.Y. Yang, Y. Zhu, X. He, Q.Y. He, Putative copper- and zinc-binding motifs in Streptococcus pneumoniae identified by immobilized metal affinity chromatography and mass spectrometry, Proteomics 11 (2011) 3288–3298.

[68]. B. Corry, Mechanisms of selective ion transport and salt rejection in carbon nanostructures, MRS Bulletin 42 (2017) 306-310.